Molecular dynamics simulation of the rotational order–disorder phase transition in calcite

2009 J. Phys.: Condens. Matter 21 095406

(http://iopscience.iop.org/0953-8984/21/9/095406)

J. Phys.: Condens. Matter **21** (2009) 095406 (11pp) doi:10.1088/0953-8984/21/9/095406

Molecular dynamics simulation of the rotational order–disorder phase transition in calcite

Jun Kawano, Akira Miyake[1], Norimasa Shimobayashi and Masao Kitamura

Department of Earth and Planetary Science, Faculty of Science, Kyoto University, Kyoto, Japan

E-mail: miya@kueps.kyoto-u.ac.jp

Received 16 December 2008
Published 30 January 2009
Online at stacks.iop.org/JPhysCM/21/095406

Abstract

Molecular dynamics (MD) simulation of calcite was carried out with the interatomic potential model based on *ab initio* calculations to elucidate the phase relations for calcite polymorphs and the mechanism of the rotational order–disorder transition of calcite at high temperature at the atomic scale. From runs of MD calculations with increasing temperature within a pressure range of 1 atm and 2 GPa, the transition of calcite with $R\bar{3}c$ symmetry into a high-temperature phase with $R\bar{3}m$ symmetry was reproduced. In the high-temperature $R\bar{3}m$ phase, CO_3 groups vibrate with large amplitudes either around the original positions in the $R\bar{3}c$ structure or around other positions rotated $\pm 60°$, and their positions change continuously with time. Moreover, contrary to the suggestion of previous investigators, the motion of CO_3 groups is not two-dimensional. At 1 atm, the transition between $R\bar{3}c$ and $R\bar{3}m$ is first order in character. Upon increasing temperature at high pressure, however, first a first-order isosymmetric phase transition between the $R\bar{3}c$ phases occurs, which corresponds to the start of $\pm 120°$ flipping of CO_3 groups. Then, at higher temperatures, the transition of $R\bar{3}c$ to $R\bar{3}m$ phases happens, which can be considered second order. This set of two types of transitions at elevated pressure can be characterized by the appearance of an 'intermediate' $R\bar{3}c$ phase between the stable region of calcite and the high-temperature $R\bar{3}m$ phase, which may correspond to the $CaCO_3$-IV phase.

1. Introduction

The existence of an order–disorder phase transition between low- and high-temperature calcite (LT- and HT-calcite) at high temperature has been suggested by a number of experiments. It has received considerable attention for the following reasons: (1) from the viewpoint of geology, calcite is a common and important mineral, and the order–disorder phase transition has a marked influence on the calcite–aragonite transition (e.g. Salje and Viswanathan 1976), and (2) calcite contains both ionic and covalent interactions, and so how CO_3^{2-} molecular ions behave in such a material is an interesting problem.

This phase transition, which occurs at 1260 K, involves an orientational disordering of the CO_3 groups upon heating. Below this temperature, the planar triangular CO_3 groups vibrate about a fixed orientation, alternate layers of CO_3 groups pointing in opposite directions, while in their high-temperature form they are orientationally disordered around their threefold axis and become equivalent. The symmetry change is from $R\bar{3}c$ to $R\bar{3}m$ with halving of the hexagonal c-axis length. This is marked by the extinction of ordered superlattice reflections, for example, 113 or 211 reflections (referred to as the hexagonal setting of the low-temperature $R\bar{3}c$ phase).

Harris (1999) summarized the experimental work of investigators such as Dove and Powell (1989), Dove *et al* (1992), Swainson *et al* (1998), and proposed that the orientational order–disorder transition is driven by large-scale continuous planar rotations of the carbonate groups. Furthermore, Harris (1999) suggested that the interactions are strongly two-dimensional in nature. However, two

[1] Author to whom any correspondence should be addressed.

Table 1. Parameter sets for the interatomic potential function (equation (1)) determined by fitting the energy surfaces calculated with *ab initio* methods.

Atom	Z (e)	A (Å)	B (Å)	C (kcal$^{1/2}$ Å^3 mol$^{-1/2}$)
O	−0.915	1.8836	0.1658	23.351
C	1.045	0.4638	0.0784	0.000
Ca	1.700	1.4466	0.1042	10.086
Atomic pair	D_1 (kJ mol^{-1})	β_1 (Å^{-1})	D_2 (kJ mol^{-1})	β_2 (Å^{-1})
O–C	45 735.0	5.14	−4936.066	2.57

molecular dynamics (MD) simulations of this phase transition (Ferrario *et al* 1994, Liu *et al* 2001) concluded that their results were consistent with the calcite-type disorder model, in which the equilibrium positions of every carbonate ion occupy the two orientations with equal probability. Moreover, Dove *et al* (2005) studied the high-temperature neutron powder diffraction of calcite and suggested that the transition is precipitated by the librational amplitude of carbonate molecular ions exceeding a critical value. However, the mechanism of the order–disorder transition is still not fully understood.

There remains another problem regarding relationships among high-temperature phases. Namely, Mirwald (1979) proposed that a stable $CaCO_3$-IV phase exists in the temperature range between the stable region of calcite and the high-temperature $R\bar{3}m$ phase. From high-temperature x-ray powder diffraction studies, he found that the thermal expansion coefficients of cell parameters change at a lower temperature than the transition temperature between the $R\bar{3}c$ and $R\bar{3}m$ phases. From this result, he proposed that these changes would signal another phase transition from calcite to $CaCO_3$–IV. However, these changes have not been detected by later experiments. Redfern *et al* (1989) considered $CaCO_3$-IV not to be a true phase, and, by applying Landau theory, concluded that the transition between $R\bar{3}c$ and $R\bar{3}m$ phases is a tricritical phase transition. By reanalyzing their data and data from other previous experiments, Harris (1999), however, cast doubt on the conclusion that this transition is tricritical. Recently, although Bagdassarov and Slutskii (2003) have observed the transformation boundary of calcite I–IV only during first-heating experiments by electrical impedance measurements in a piston–cylinder apparatus, this phase transition remains difficult to identify.

In this study, we used MD simulation to elucidate the phase relations among LT-calcite, HT-calcite, and calcite-IV, and the transition mechanism at high temperature. Here, each atom is treated independently and all interactions are described with one interatomic potential function between every two atoms, which is different from the previous model that treated the CO_3^{2-} group as a rigid molecular ion (Ferrario *et al* 1994). Furthermore, the pressure dependence of the phase relations, which had not been focused on previously, was elucidated by calculations that simulate high-pressure conditions.

2. Interatomic potential

The interatomic potential function (ϕ_{ij}) for MD calculations between two atoms (the ith and jth atoms) is given by the following equation:

$$\phi_{ij}(r_{ij}) = \frac{z_i z_j e^2}{r_{ij}} + f_0(B_i + B_j)\exp\frac{A_i + A_j - r_{ij}}{B_i + B_j} - \frac{C_i C_j}{r_{ij}^6} + D_{1ij}\exp(-\beta_{1ij} r_{ij}) + D_{2ij}\exp(-\beta_{2ij} r_{ij}), \quad (1)$$

which consists of the Coulombic interaction between point charges, short range repulsion, van der Waals attraction, and Morse potential terms; and where r_{ij} is the interatomic distance between the ith and jth atoms, $f_0 = 6.9511 \times 10^{-11}$ N is a constant, e is the electronic charge, z, A, B, and C are the parameters for each atomic species, and D_1, D_2, β_1, and β_2 are the parameters for the C–O pair. In this study, the parameter sets were obtained by fitting to the potential surface simulated by quantum-mechanical calculations. All quantum-mechanical computations were performed with CRYSTAL98 code (Saunders *et al* 1999), which is based on the theory of one-electron self-consistent-field equations for a periodic system, and uses localized basis functions (linear combinations of atomic orbitals, LCAO) with Hartree–Fock (HF) Hamiltonians. The basis sets utilized for Ca, C, and O in the previous study (Catti and Pavese 1997) were used. The fitted potential energy surfaces for the bulk crystal of calcite were then obtained by changing the structure parameters from the optimized structure with seven different modes, which consist of three structural modes: (a) stretching the hexagonal a-axis while retaining the C–O bond length, (b) stretching the hexagonal c-axis, and (c) changing the volume while keeping the c/a ratio and C–O bond length constant; and four modes of the CO_3^{2-} ion: (d) stretching all the C–O bonds while maintaining D_{3h} symmetry, which corresponds to symmetric stretching and is denoted by ν_1 in Herzberg's conventions (Herzberg 1945), (e) movement of O atoms along the c-axis while maintaining the C_{3v} symmetry of the CO_3^{2-} ion, which corresponds to out-of-plane bending of the CO_3^{2-} ion (ν_2 in Herzberg's conventions), (f) movement of the CO_3^{2-} ion along the c-axis while keeping the threefold axis, and (g) rotation of the CO_3^{2-} ion around the c-axis while keeping the threefold axis. Table 1 shows the parameter sets derived by this method.

3. Molecular dynamics (MD) calculations

Using the newly derived potential parameters, MD calculations were carried out with the MD program MXDTRICL (Kawamura 1997). The Ewald method was applied for the summation of Coulombic interactions, and the equations of motions were integrated by Verlet's algorithm with a time step

Table 2. Structural parameters determined from our MD calculations and the experimental data obtained by Effenberger *et al* (1981).

	MD	Obs.
a_{h1} (Å)	5.049	4.9896
a_{h2} (Å)	5.049	4.9896
c_h (Å)	17.767	17.061
V (Å^3)	392.26	367.846
ρ (g cm^{-3})	2.54	2.71
C–O (Å)	1.2716	1.2813

of 0.5 fs. The temperatures and pressures were controlled by scaling the particle velocities and adjusting the cell parameters, respectively. Periodic boundary conditions were imposed by the MD basic cell.

The unit cell adopted in our MD simulation (MD cell) was composed of 72 crystallographic unit cells of calcite ($a_{\mathrm{MD}} = 6a$, $c_{\mathrm{MD}} = 2c$, in the hexagonal setting), containing 2160 atoms. The MD simulation was started from a relaxed structure, which was obtained by annealing at 300 K and 1 atm for a sufficiently long time using the experimentally obtained structure of Wyckoff (1963) as the initial structure. Then the temperature was increased to 1300 K at 1 atm using the calculated relaxed structure as the starting structure. Furthermore, heating runs were also carried out under high-pressure conditions (1 and 2 GPa). For each heating run, the pressure was first elevated to the appropriate value at 300 K, and then the temperature was varied at constant pressure from 300 to 1600 K using the calculated structure at 300 K as the initial structure.

The crystallographic and thermodynamic properties reported in this study were derived from time averages taken over a sufficiently long time (at least 10 ps = 20 000 steps) after annealing at each P–T condition (for at least 10 ps). The diffracted intensity was calculated from the structure factor obtained directly from the MD-simulated atomic positions by using a program developed by Miyake *et al* (1998). The power spectrum for each atom was obtained by Fourier transformation of its velocity autocorrelation function.

4. Results and discussion

4.1. MD-simulated structure at 300 K and atmospheric pressure

We compared the structural parameters derived from the MD-simulated structure of calcite at 300 K and atmospheric pressure with those determined by an x-ray diffraction method (table 2). For our simulation, we employed a parallelepiped MD cell and did not impose rhombohedral or hexagonal symmetry on the MD-simulated crystal. The lengths of the a_1- and a_2-axes were therefore not exactly equal and the angles between the crystallographic axes were not fixed in the calculations. As can be seen in table 2, the cell parameters at 300 K show good agreement (within about 6%) with those of a real crystal.

The vibrational spectra of O and C atoms are shown in figure 1. It has been reported that there are four modes of CO_3 groups in this wavenumber range. Herzberg (1945) assigned the notation ν_1–ν_4 to these modes. In the present calculation, only O atoms vibrate in the x–y plane in the mode at around 1100 cm^{-1}, as shown in figure 1. Therefore, this mode is considered to be symmetric stretching of the CO_3 ion, which corresponds to Herzberg's ν_1 mode. Next, each ion vibrates along the z direction only in the mode at around 840 cm^{-1}. This is a feature of out-of-plane bending, corresponding to the ν_2 mode. The other two modes are asymmetric. In the mode at around 1200 cm^{-1}, mainly C atoms are vibrating, whereas at the 730 cm^{-1} mode O atoms are vibrating. These results show that the former corresponds to Herzberg's ν_3 mode, and the latter to the ν_4 mode. By comparing the wavenumber of each mode with the results from IR and Raman spectroscopy (table 3), we concluded that the sequence of the peaks for the vibrational modes of the CO_3^{2-} ion was reproduced successfully. In particular, the symmetric stretching (at about 1100 cm^{-1}) and the out-of-plane bending (at about 880 cm^{-1}) of the CO_3^{2-} ion were reproduced very well.

Table 3. Calculated vibrational frequencies of the four modes of CO_3, together with the infrared (ν_2–ν_4) and Raman (ν_1) data from White (1974) for comparison (ν_1–ν_4 are Herzberg's conventions). ν_1 and ν_2 marked with * are the modes fitted to the potential surfaces obtained by *ab initio* calculations.

	ν (cm^{-1})	ν_1^* (cm^{-1})	ν_2^* (cm^{-1})	ν_4 (cm^{-1})
MD.	1200	1100	840	730
Obs.	1407	1088	872	712

4.2. Temperature dependence of an MD-simulated crystal at 1 atm

The change of the lattice constants and the unit cell volume at 1 atm as a function of temperature is shown in figure 2, where experimental results of Markgraf and Reeder (1985) are also presented for comparison. The results show that the thermal expansion is anisotropic. Although the c-axis length increases rapidly with temperature, the a-axis length does not change remarkably. This tendency of the thermal expansion is consistent with the experimental results.

From 1200 to 1250 K, the changes of the parameter c and the unit cell volume show discontinuities. Furthermore, the relative intensity of the 113–104 reflections decreases gradually upon increasing temperature and abruptly disappears between 1200 and 1250 K (figure 3). These results indicate that the 113 reflection disappears above 1200 K while the 104 reflection appears over the entire temperature range; therefore, the transition from $R\bar{3}c$ to $R\bar{3}m$ occurs between 1200 and 1250 K. The temperature at which the volume increases markedly and the intensity of the reflection 113 vanishes is taken to be the transition temperature, and is denoted as T_c.

The orientational distribution of the angle from the a-axis of the C–O bonds is considered at each temperature. Figure 4 shows the probability distribution function $P(\phi)$ of the angle ϕ between the a-axis and the C–O bonds in the same a–b plane. Below 1200 K, O atoms vibrate very close to the equilibrium sites of $R\bar{3}c$ symmetry, where the angular distribution has

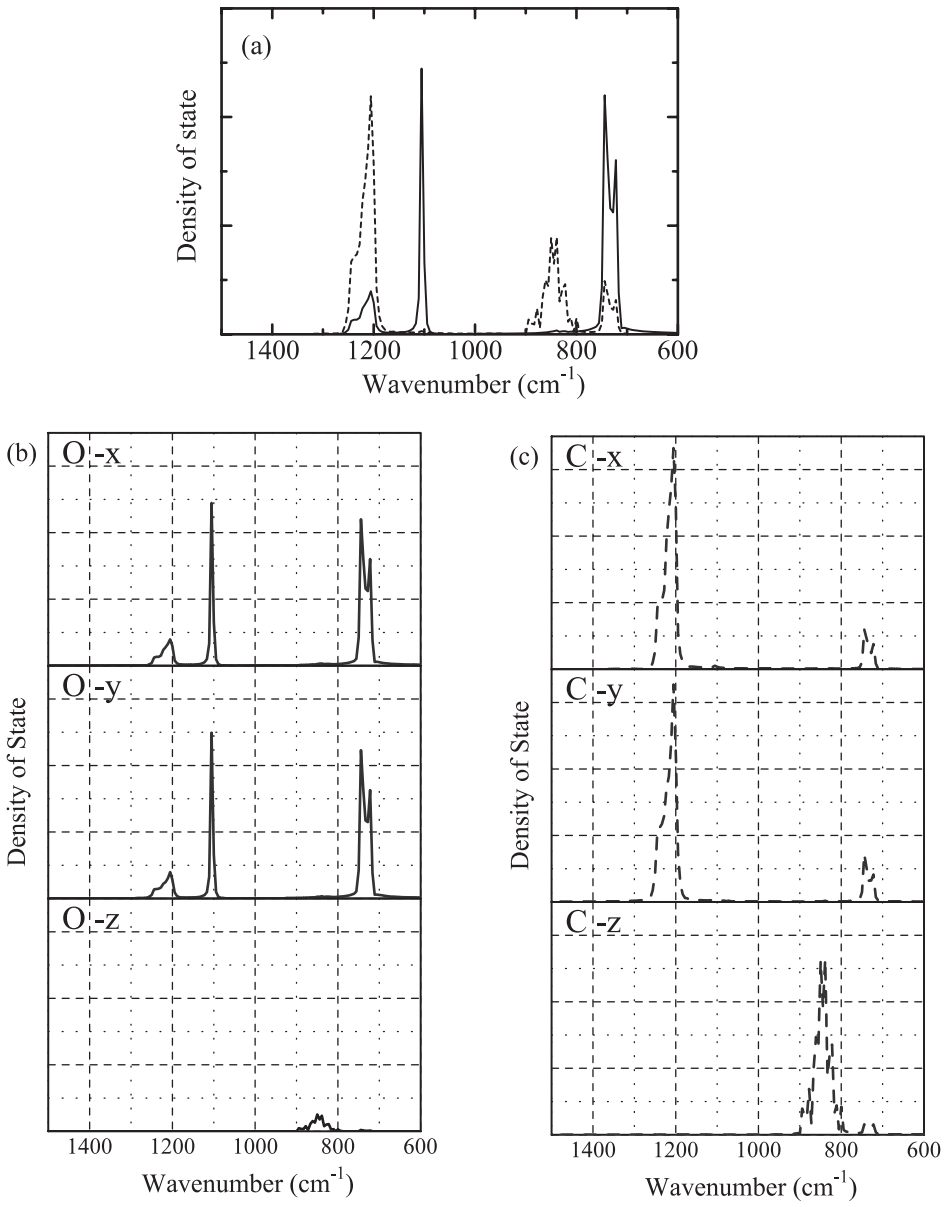

Figure 1. (a) Power spectra of calcite obtained by MD calculations at 300 K and 1 atm. The spectrum for O atoms is shown by the solid line, and for C atoms by the dashed line. The vibrational spectra in each of the x, y, and z directions for O and C atoms are shown separately in (b) and (c), respectively.

maxima at 60°, 180°, and 300° from the a-axis, and the atoms have a probability of 0 for vibrating at around 0°, 120°, and 240°. Above 1250 K, however, $P(\phi)$ has maxima not only at about 60°, 180°, and 300°, but also at around 0°, 120°, and 240°, and CO_3 groups exist at these positions with equal probability. This means the two orientational positions of CO_3 groups (i.e. the equilibrium position of $R\bar{3}c$ symmetry and the position rotated by ±60°) become equivalent, which is consistent with the $R\bar{3}m$ structure. To consider the behavior of an individual CO_3 group, the rotation angle with time at 1200 and 1250 K of one of the CO_3 groups is shown in figure 5. Even at just below the transition temperature, 1200 K, CO_3 vibrates at around one equilibrium position. Above 1250 K, CO_3 sometimes 'flips' ±60° from the original position and changes direction.

Next, we consider the libration of CO_3 groups out of the a–b plane (figure 6(a)). The distribution of the angle between one of the C–O bonds in a CO_3 group and the a–b plane is shown in figure 6(b). This figure shows that the amplitude of CO_3 groups becomes larger as the temperature increases, although they remain in the a–b plane on average. From the standard deviation of the libration angle as a function of temperature, we can see that the amount of libration of CO_3 groups out of the a–b plane increases with temperature and increases markedly at the transition temperature T_c (figure 6(c)). Below T_c, CO_3 groups stay at the equilibrium position of the $R\bar{3}c$ structure, and vibrate both in and out of the a–b plane more intensely with increasing temperature. When the temperature reaches T_c, they are able to climb over the 'barrier' and rotate

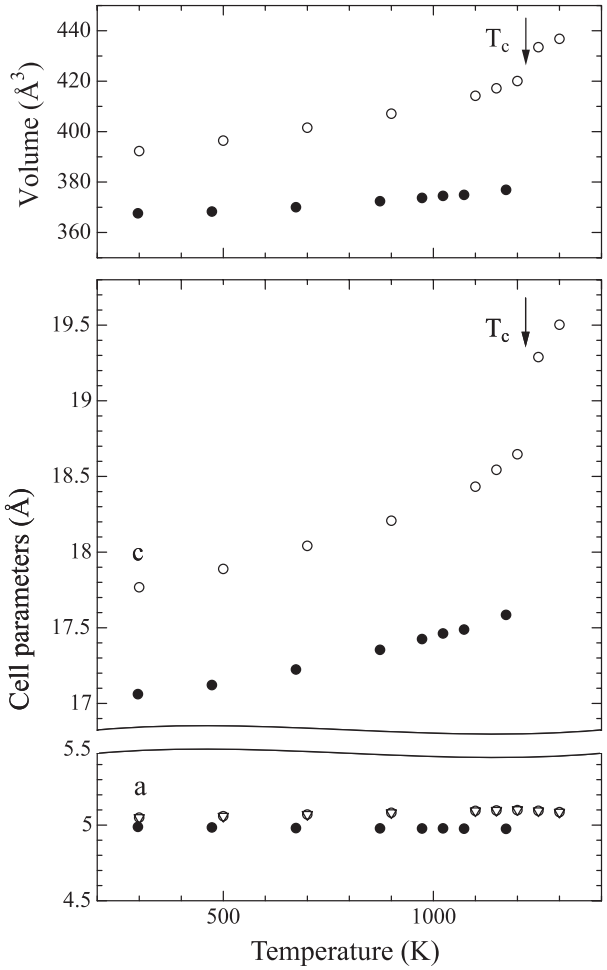

Figure 2. Temperature dependencies of cell parameters and the unit cell volume of MD-simulated calcite at 1 atm. The simulated values of our study are shown by open circles (○) and triangles (▽), together with experimental values from Markgraf and Reeder (1985), shown by closed circles (●).

±60° into the next equilibrium position, which causes the transition.

In the high-temperature structure above T_c, CO_3 groups vibrate with large amplitude at around either the original position in the ordered structure or another position rotated ±60°, and change their positions with time.

4.3. Temperature dependence of MD-simulated crystals at elevated pressures

The temperature dependencies of the lattice constants at 1 and 2 GPa are summarized in figure 7. The changes of the *c*-axis and the molar volume also have slight but definite discontinuities under each pressure condition. In figure 7, the temperature at which the *c*-axis and molar volume change discontinuously is identified with an arrow as T_1. At 2 GPa, the degree of discontinuity of the molar volume change at T_1 seems to become smaller as the temperature increases. In addition, at the same temperature T_1, the gradient of the change of the *a*-axis length turns from positive to negative.

As shown in figure 8, the relative intensity of the 113 reflection decreases gradually with increasing temperature and

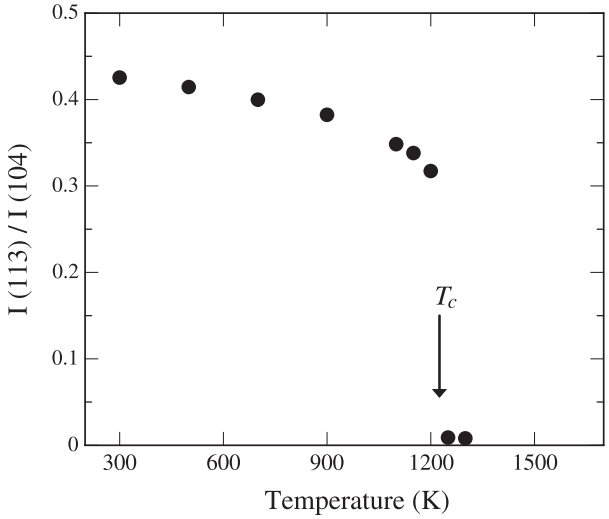

Figure 3. Temperature dependence of the ratio of the intensity of 113–104 reflections in MD-simulated calcite at 1 atm (in hexagonal setting). The transition temperature T_c is shown by an arrow.

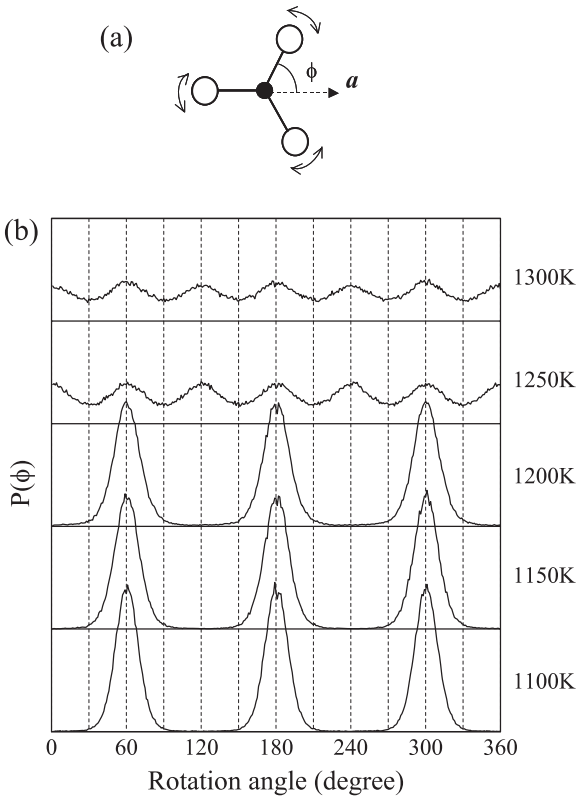

Figure 4. (a) Schematic drawing of the rotation angle ϕ between the *a*-axis and the C–O bonds in the CO_3 group. (b) Temperature dependence of the probability distribution function $P(\phi)$ for the angle ϕ in the same plane at 1 atm.

finally vanishes. This result indicates that the transition to $R\bar{3}m$ also exists. However, the transition temperature where that reflection vanishes, denoted here as T_2, is not the same as T_1. In figure 7, T_1 and T_2 are shown by arrows together with the cell parameter changes. Particularly in the case of 1 GPa, a slight discontinuity in the relative intensity change of

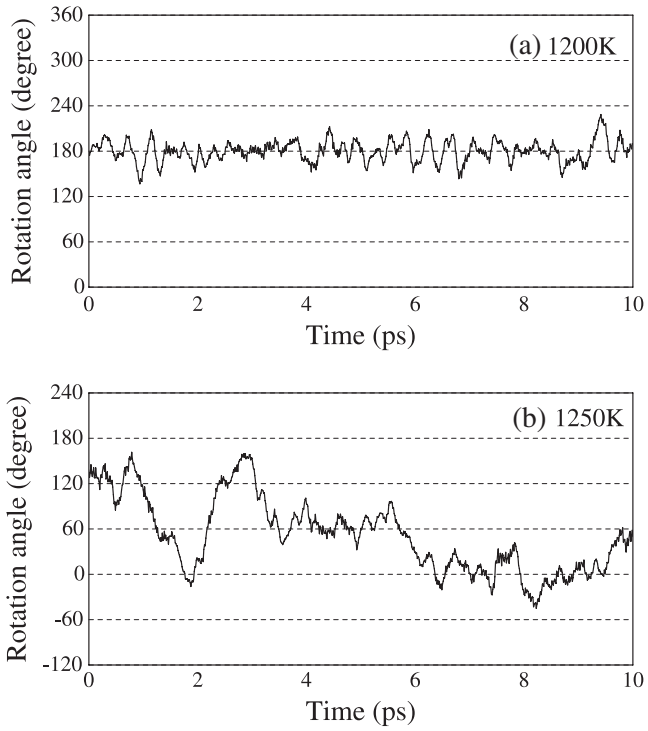

Figure 5. Time dependence at 1 atm of the angle between one C–O bond and the *a*-axis at (a) 1200 K and (b) 1250 K.

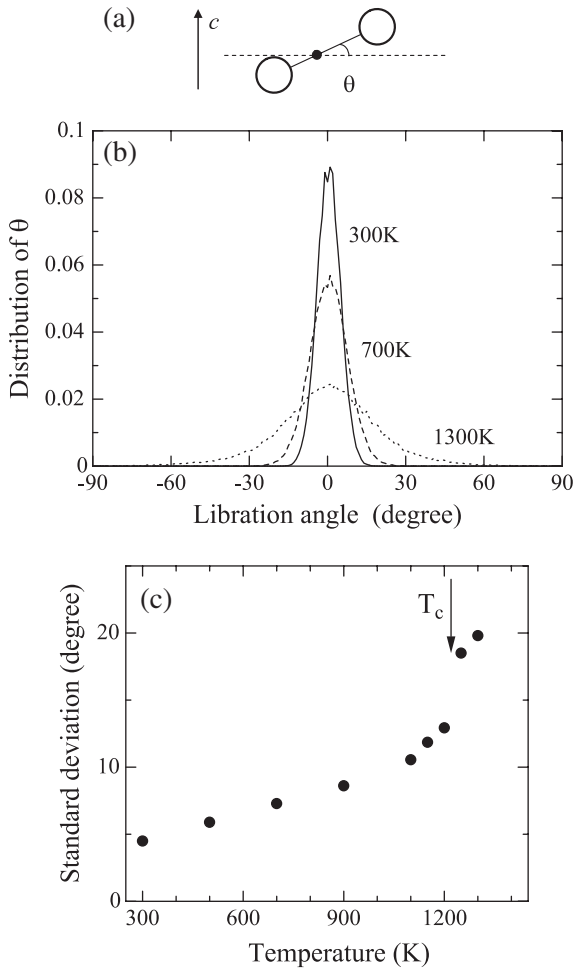

Figure 6. (a) Schematic drawing of CO_3 libration by an angle θ out of the *a*–*b* plane. (b) The probability distribution of θ between one C–O bond of CO_3 and the *a*–*b* plane at 1 atm for three temperature conditions. (c) Temperature dependence of the standard deviation of the probability distribution of θ. Transition temperature T_c is shown with an arrow.

the 113 reflection can be observed at T_1. This means that there are two types of transitions: at T_1, a transition occurs between two phases that have the same space group $R\bar{3}c$, whereas at a slightly higher temperature T_2, a transition from $R\bar{3}c$ to $R\bar{3}m$ occurs.

The orientational angular distributions of the C–O bonds change as follows.

(1) Below T_1, all of the O atoms vibrate at the equilibrium positions of $R\bar{3}c$ symmetry at 60°, 180°, and 300° from the *a*-axis (figure 9). As the temperature increases, they vibrate more intensively in the *a*–*b* plane, which makes the gradient of the change of the *a*-axis length smaller.

(2) At T_1, CO_3 groups start flipping ±120°, which makes the volume increase discontinuously and leads to the phase transition. Between T_1 and T_2, the maxima of the orientational distribution of the C–O bonds are still at 60°, 180°, and 300°, however, it becomes possible for the C–O bonds to exist at any orientation. To study the rotation of an individual CO_3 ion at 2 GPa, the variation of the rotation angle of one CO_3 group with time is shown in figure 10. At 1450 K, a temperature between T_1 and T_2, the CO_3 group seems to stay at an equilibrium position of $R\bar{3}c$ symmetry, but it sometimes changes direction to a position rotated ±120° from the original direction (figure 10(a)). In the structure between T_1 and T_2, CO_3 groups switch positions by ±120° rotations over time, but these are the equilibrium positions of an ordered phase. Therefore, the symmetry of the structure is still $R\bar{3}c$, and the transition occurring at T_1 is the isosymmetric transition between two phases that have the same $R\bar{3}c$ space group. This transition at elevated pressure can be characterized by the appearance of an 'intermediate' $R\bar{3}c$ phase between T_1 and T_2, different from the transition at 1 atm.

(3) Above T_2, the distribution begins to have maxima not only at about 60°, 180°, and 300°, but also at around 0°, 120°, and 240°, which leads to the transition to the high-temperature $R\bar{3}m$ phase. In addition, a considerable number of C–O bonds also exist in this stage between these equilibrium sites, i.e. at 30°, 90°, 150°, 210°, 270°, and 330° (figure 9). The variation of rotation angle of one CO_3 group with time at 1500 K (figure 10(b)) suggests that CO_3 groups rotate continuously and do not stay for a long time at these equilibrium positions in the high-temperature $R\bar{3}m$ phase. Consequently, CO_3 groups come to exist both at the original $R\bar{3}c$ positions and the ±60° rotated positions with the same probability, which leads to the extinction of the 113 reflection and the occurrence of the transition from $R\bar{3}c$ to $R\bar{3}m$.

Although Liu *et al* (2001) predicted that the transition from $R\bar{3}c$ to $R\bar{3}m$ would be a calcite-type disorder originating only from the orientational distribution of CO_3 groups, we cannot simply conclude that this transition can be explained by

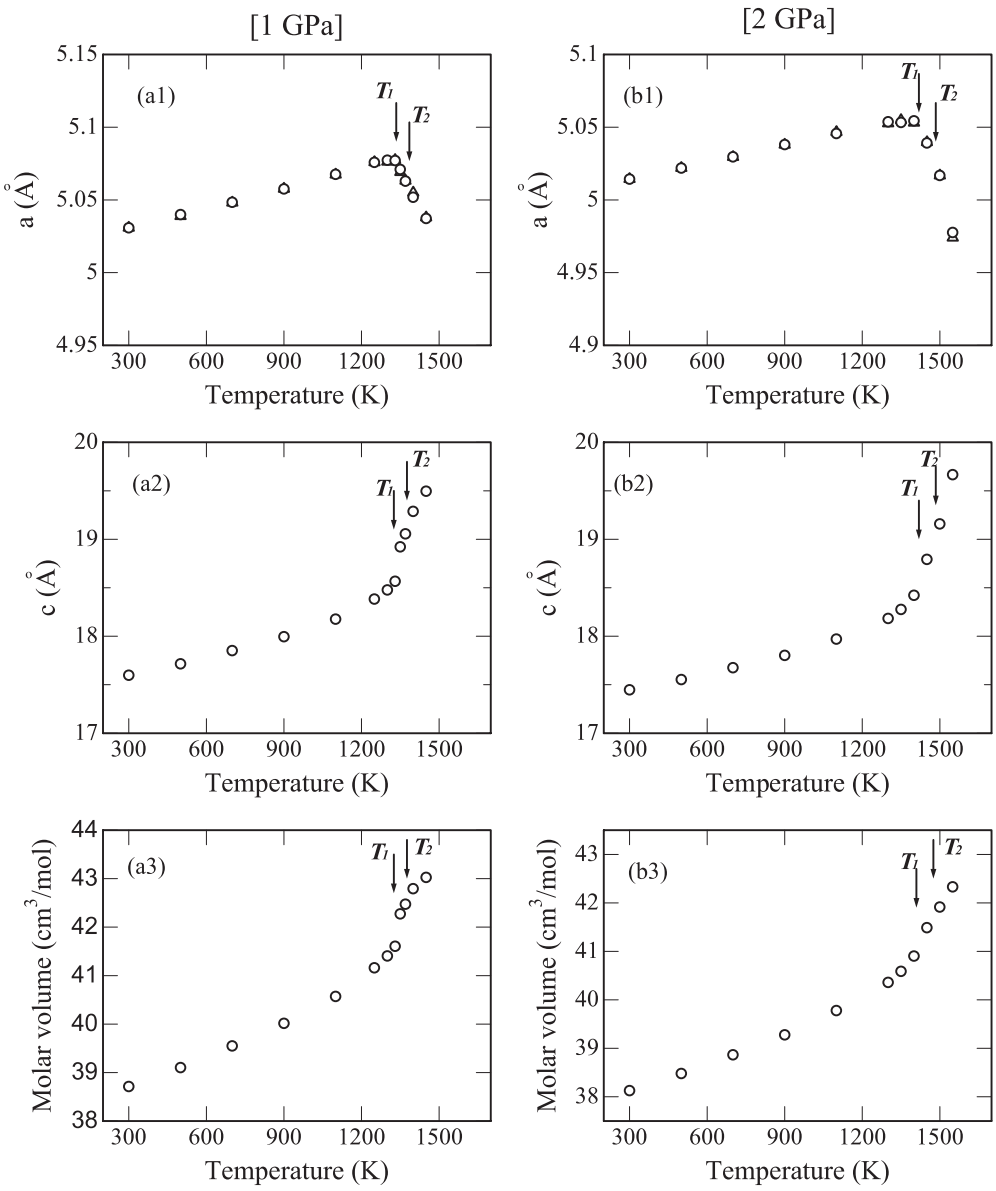

Figure 7. Temperature dependencies of the cell parameters and the molar volume at (a1-3) 1 GPa and (b1-3) 2 GPa. The temperature T_1 at which the thermal expansion coefficient of each cell parameter changes, and the transition temperature T_2 determined by the extinction of the intensity of the 113 reflection, are shown with arrows.

this type of disorder. Instead, we suppose that this transition should be a mixed type between calcite-type ordering and continuous planar rotation.

Next, we discuss the dimensional behavior of CO_3 groups. Harris (1999) suggested that the behavior of CO_3 groups is strongly two-dimensional. However, our model indicates that the transition occurs only when CO_3 groups librate so intensely out of the *a*–*b* plane as to climb up the 'barrier' at high temperature. Moreover, as seen in figures 2 and 6, the variation trend of the libration of CO_3 groups is similar to the tendency of the temperature dependency of the crystallographic *c*-axis length, which indicates that the thermal expansion of the *c*-axis is strongly affected by CO_3 libration along the *c*-axis. These results indicate that the libration of CO_3^{2-} ions along the *c*-axis is more important than was considered in previous studies.

4.4. Phase relationship

To elucidate the phase relations at high temperature, the results of our calculations are summarized in a *P*–*T* diagram (figure 11). The transition temperature at 1 atm is between 1200 and 1250 K. Because the change of the cell parameters and the intensity of the 113 reflection as functions of temperature have obvious discontinuities at the transition temperature, the transition can be considered to be first order at 1 atm.

With heating at elevated pressure, first an isosymmetric phase transition between $R\bar{3}c$ phases occurs at T_1. Because this transition involves a discontinuous change of the volume and intensity of the 113 reflection (figure 8), it is first order in character. This transition corresponds to the start of $\pm 120°$ flipping of the CO_3 groups. Then, at higher temperature T_2,

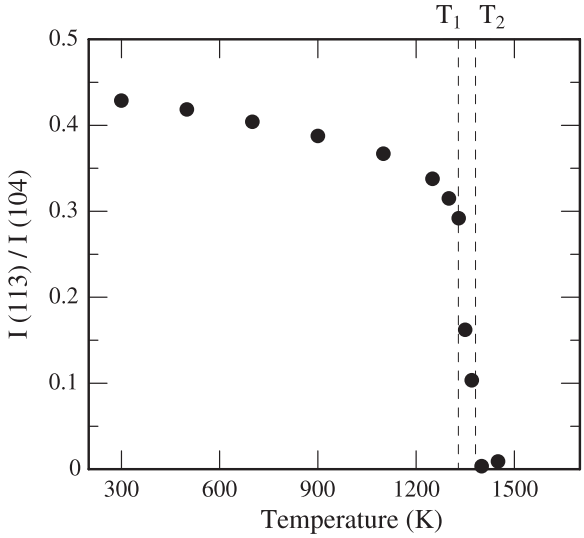

Figure 8. Temperature dependence of the relative intensity of the 113–104 reflections of MD-simulated calcite at 1 GPa. The ratio of the intensities changes discontinuously at T_1 and vanishes at T_2.

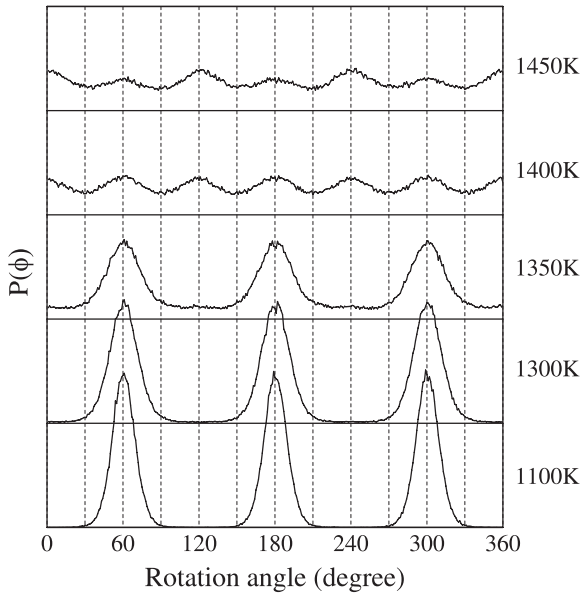

Figure 9. Temperature dependence of the probability distribution function $P(\phi)$ for the angle ϕ between the a-axis and the C–O bonds in the same plane at 1 GPa.

the transition of $R\bar{3}c$ to $R\bar{3}m$ phases happens, which can be considered to be second order because the intensity of the 113 reflection decreases continuously from T_1 and finally vanishes at T_2 (figure 8). Furthermore, the volume change becomes more continuous as the pressure increases. Therefore, at pressures higher than those of our simulations, it is possible that the transition between $R\bar{3}c$ and $R\bar{3}m$ phases is continuous. These two types of equilibrium lines are shown in figure 11. Both of the slopes of these transitions $\mathrm{d}P/\mathrm{d}T$ are positive and become steeper with increasing pressure. Moreover, the separation between these two lines becomes larger with increasing pressure.

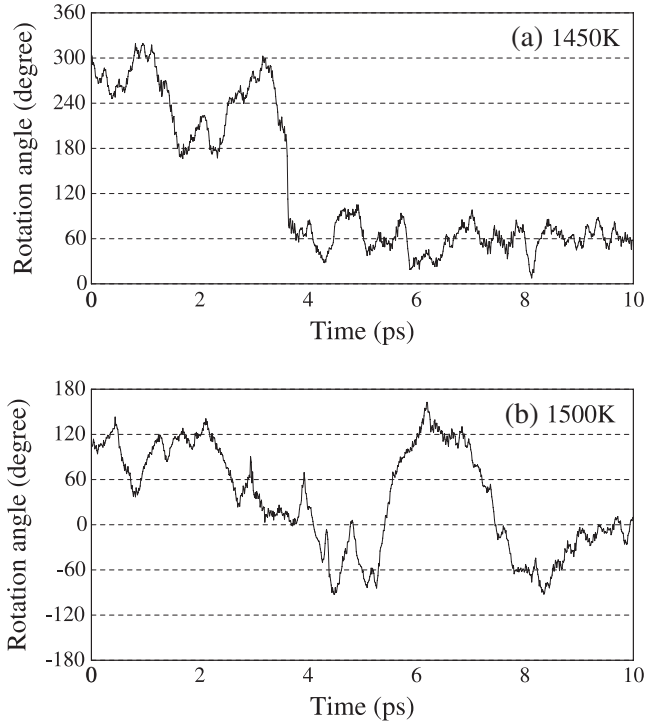

Figure 10. Time dependence at 2 GPa of the angle between one C–O bond and the a-axis at (a) 1450 K and (b) 1500 K.

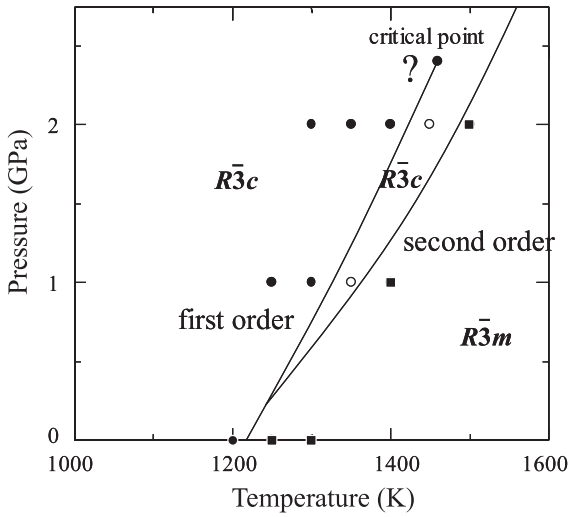

Figure 11. Phase diagram for $R\bar{3}c$ and $R\bar{3}m$ phases obtained by our MD calculations at high temperature. Closed circles indicate the low-temperature calcite ($R\bar{3}c$) structure in which CO_3 groups that do not rotate appear, open circles represent the $R\bar{3}c$ structure in which CO_3 groups flip $\pm 120°$ with time, and squares indicate $R\bar{3}m$ structure. Two phase boundaries are shown: one represents the equilibrium line of the first-order transition between $R\bar{3}c$ phases, which has a critical point, and the other shows the equilibrium line of the second-order transition between $R\bar{3}c$ and $R\bar{3}m$ phases. At 1 atm, only the first-order transition between $R\bar{3}c$ and $R\bar{3}m$ phases occurs.

Generally, transitions between two phases that have the same space groups have been reported to have a critical point at which the equilibrium line terminates (Christy 1995). Thus, also in the present case, the equilibrium line of the first-

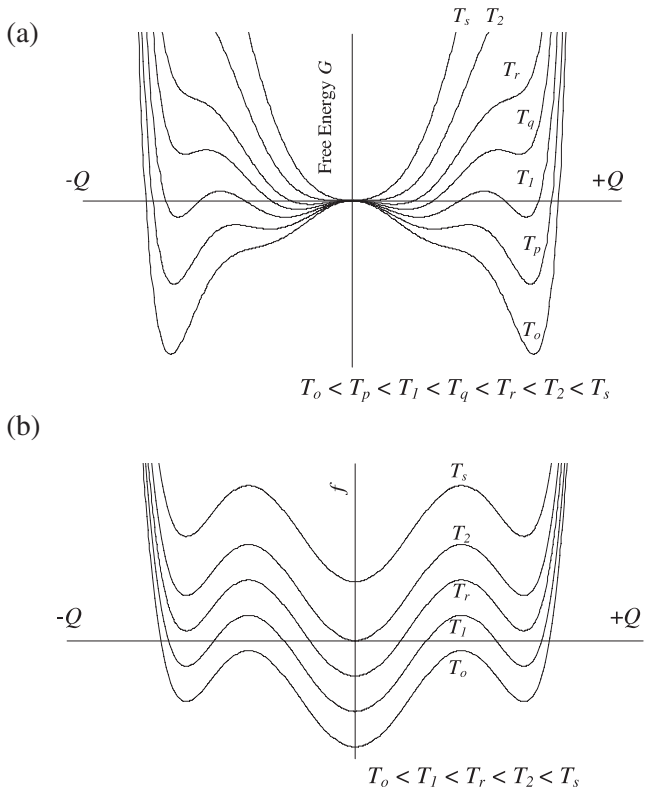

Figure 12. (a) Temperature dependence of the excess free energy G as a function of the order parameter Q. The tendency of these curves shows the set of first-order and second-order phase transitions, and T_1 and T_2 are the transition temperatures for first- and second-order transitions, respectively. These curves correspond to the eighth-order expansion of Q (equation (2)), where $b = 11$, $c = -6$, $d = 1$ in all curves, and $a = 9$ at T_o, 7.5 at T_p, 6 at T_1, 4.5 at T_q, 3 at T_r, 0 at T_2, and 5 at T_s. (b) Temperature dependence of the function f (see equation (4)) derived from $\mathrm{d}G/\mathrm{d}Q$. Each temperature corresponds to the same value of a as that in (a).

order transition between $R\bar{3}c$ phases could possibly terminate at the critical point. At pressures higher than that point, an isosymmetric transition between $R\bar{3}c$ phases does not occur and the low-temperature $R\bar{3}c$ phase transforms continuously to the high-temperature $R\bar{3}m$ phase by a second-order transition. Although the P–T condition of the critical point could not been determined from our calculations, the critical point is added schematically to figure 11.

The excess free energy G due to this set of first-order and second-order phase transitions can be described by an eighth-order expansion of the order parameter Q following Landau theory (figure 13(a)). Namely,

$$G = aQ^2 + bQ^4 + cQ^6 + dQ^8, \tag{2}$$

where a, b, c, and d are coefficients. This transition shows the following features in the range $Q > 0$ as the temperature increases ($T_o < T_p < T_1 < T_q < T_r < T_2 < T_s$).

(1) At low temperature (T_o in figure 12(a)), the free energy G has only one energy minimum.
(2) At T_p, another local minimum for the less stable phase appears at lower Q, and there are two local minima.
(3) At T_1, two local minima have the same value, and there is a jump in Q from the larger local minimum to the smaller one. This means that a first-order transition occurs.
(4) At T_q, there are still two local minima, and Q for the stable phase is the smaller one.
(5) At T_r, the local minimum for the less stable phase disappears, and Q for the stable phase gradually approaches zero.
(6) At T_2, the minimum other than zero disappears, and Q reaches zero. This is a second-order transition.

Now let us consider the derivative of G with respect to Q:

$$\begin{aligned}\mathrm{d}G/\mathrm{d}Q &= 2aQ + 4bQ^3 + 6cQ^5 + 8dQ^7 \\ &= Q(2a + 4bQ^2 + 6cQ^4 + 8dQ^6).\end{aligned} \tag{3}$$

If the following definition is invoked:

$$f \equiv 2a + 4bQ^2 + 6cQ^4 + 8dQ^6, \tag{4}$$

the features of the set of transitions described above are achieved when the equation $f = 0$ has one real root around T_o, three roots between T_p and T_q, one root around T_r, and no real root above T_2. To satisfy this tendency, at least the coefficient a should increase with increasing temperature, which does not affect the shape of the curve, but does affect the position as shown in figure 12(b). Actually, figure 12(a)

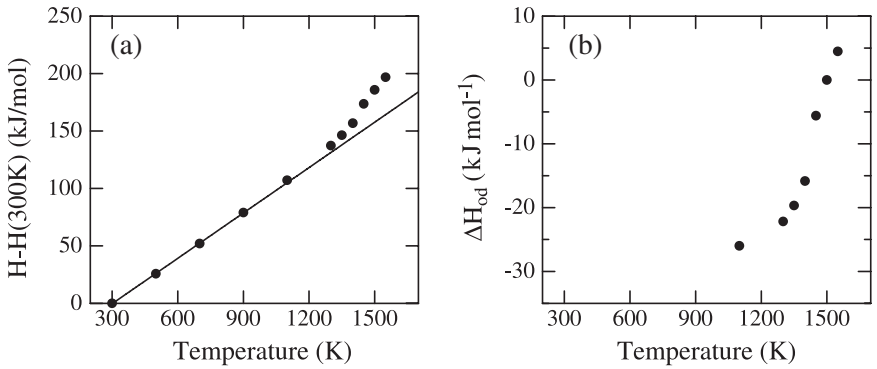

Figure 13. (a) Temperature dependence of the enthalpy at 2 GPa, shown as the difference from the enthalpy at 300 K. The extrapolation of the low-temperature data between 300 and 900 K is shown by the solid line. (b) Temperature dependence of the excess enthalpy at 2 GPa, expressed by the difference from the extrapolation of the low-temperature data.

shows the changes in the free-energy curve for the case in which only the coefficient a increases. That is, a should have a negative value at low temperature and increase as the temperature increases. Then, the first-order phase transition at T_1 occurs when $8ad^2 - 4bcd + c^3 = 0$, which is the condition when the two minima have the same value and is derived by Christy's analysis (Christy 1995). After that, the second-order transition at T_2 happens when $a = 0$, and a should be positive above T_2.

Some previous experimental results suggest that this transition between $R\bar{3}c$ and $R\bar{3}m$ phases shows features of a tricritical phase transition (Redfern *et al* 1989, Dove and Powell 1989). For example, Redfern *et al* (1989) analyzed excess enthalpy ΔH_{od} data by using Landau theory, and concluded this could be a tricritical phase transition. The excess enthalpy ΔH_{od} obtained in our calculations at 2 GPa (figure 13) has a trend similar to the results of Redfern *et al* (1989), however, detailed analysis reveals that two types of phase transition occur. Namely, a first-order isosymmetric transition between $R\bar{3}c$ phases at T_1 and a second-order transition between $R\bar{3}c$ and $R\bar{3}m$ phases at T_2. It is possible that the $CaCO_3$-IV phase previously proposed by Mirwald (1979) is related to the 'intermediate' $R\bar{3}c$ phase that appears in our calculations between T_1 and T_2.

5. Summary

As a result of our MD calculations with a newly derived model, we propose that the transition of calcite to the high-temperature phase proceeds as follows:

Transition at 1 atm

Below the transition temperature, CO_3 groups vibrate both in and out of the a–b plane more intensely as the temperature increases, at around the equilibrium positions of the $R\bar{3}c$ structure. When the transition temperature is reached, they are able to climb over the 'barrier' and rotate $\pm 60°$ into the next equilibrium position, which causes the discontinuous transition to $R\bar{3}m$. In the high-temperature phase, CO_3 groups change with time between the original position in the ordered structure and another position rotated $\pm 60°$, with large-amplitude vibrations.

Transition at higher pressures

(1) Below the transition temperature, CO_3 groups vibrate at the equilibrium positions of the $R\bar{3}c$ phase.
(2) Upon heating, CO_3 groups start flipping $\pm 120°$ at T_1, which makes the volume increase discontinuously, leading to the phase transition. Between T_1 and T_2, CO_3 groups switch positions by $\pm 120°$ rotations with time, but these positions are the equilibrium positions of an ordered phase. Therefore, the symmetry of the structure is still $R\bar{3}c$.
(3) Above temperature T_2, CO_3 groups rotate continuously and exist at both the original $R\bar{3}c$ positions and the $\pm 60°$ rotated positions with the same probability, which leads to the transition from $R\bar{3}c$ to $R\bar{3}m$.

Thus, the transition between $R\bar{3}c$ and $R\bar{3}m$ is first order in character at 1 atm. Upon heating at high pressure, the first-order isosymmetric phase transition between $R\bar{3}c$ phases occurs first, and then the second-order transition of $R\bar{3}c$ to $R\bar{3}m$ phases happens at a higher temperature.

Acknowledgments

We are grateful to K Kawamura and T Tsuchiya for important advice concerning the calculations. This work was partly supported by a Grant-in-Aid for Scientific Research from the Ministry of Education, Science, Sports, and Culture in Japan.

References

Bagdassarov N S and Slutskii A N 2003 Phase transformations in calcite from electrical impedance measurements *Phase Transit.* **76** 1015–28
Catti M and Pavese A 1997 Quantum-mechanical and classical simulations of Mg–Ca carbonates *Modelling of Minerals and Silicate Materials* ed B Silvi and P D'Arco (Dordrecht: Kluwer–Academic) pp 113–56
Christy A G 1995 Isosymmetric structural phase transition: phenomenology and examples *Acta Crystallogr.* B **51** 753–7
Dove M T, Hagen M E, Harris M J and Powell B M 1992 Anomalous inelastic neutron scattering from calcite *J. Phys.: Condens. Matter* **4** 2761–74
Dove M T and Powell B M 1989 Neutron diffraction study of the tricritical orientational order/disorder phase transition in calcite at 1260 K *Phys. Chem. Minerals* **16** 503–7
Dove M T, Swainson I P, Powell B M and Tennant D C 2005 Neutron powder diffraction study of the orientational order–disorder phase transition in calcite, $CaCO_3$ *Phys. Chem. Minerals* **32** 493–503
Effenberger H, Mereiter K and Zemann J 1981 Crystal structure refinements of magnesite, calcite, rhodochrosite, siderite, smithsonite and dolomite, with discussion of some aspects of the stereochemistry of calcite type carbonates *Z. Kristallogr.* **156** 233–43
Ferrario M, Lynden-Bell R M and McDonald I R 1994 Structural fluctuations and the order–disorder phase transition in calcite *J. Phys.: Condens. Matter* **6** 1345–58
Harris M J 1999 A new explanation for the unusual critical behavior of calcite and sodium nitrate, $NaNO_3$ *Am. Mineral.* **84** 1632–40
Herzberg G 1945 *Infrared and Raman Spectra of Polyatomic Molecules* (New York: Van Nostrand)
Kawamura K 1997 MXDTRICL *Japan Chemical Program Exchange,* #77
Liu J, Duan C-G, Ossowski M M, Mei W N, Smith R W and Hardy J R 2001 Simulation of structural phase transition in $NaNO_3$ and $CaCO_3$ *Phys. Chem. Minerals* **28** 586–90
Markgraf S A and Reeder R J 1985 High-temperature structure refinements of calcite and magnesite *Am. Mineral.* **70** 590–600
Mirwald P W 1979 Determination of a high-temperature transition of calcite at 800 °C and one bar CO_2 pressure *Neues Jahrbuch Mineralogie, Mönatshefte* **7** 309–15
Miyake A, Hasegawa H, Kawamura K and Kitamura M 1998 Symmetry and its change in a reciprocal space of a quartz crystal simulated by molecular dynamics *Acta Crystallogr.* A **54** 330–7
Redfern S A T, Salje E and Navrotsky A 1989 High-temperature enthalpy at the orientational order–disorder transition in calcite: implications for the calcite/aragonite phase equilibrium *Contrib. Mineral. Petrol.* **101** 479–84

Salje E and Viswanathan K 1976 The phase diagram calcite-aragonite as derived from the crystallographic properties *Contrib. Mineral. Petrol.* **55** 55–67

Saunders V R, Doves R, Roetti C, Causá M, Harrison N M, Orlando R and Zilcovich-Wilson C M 1999 *CRYSTAL98 User's Manual* (Torino: University of Torino)

Swainson I P, Dove M T and Harris M J 1998 The phase transitions in calcite and sodium nitrate *Physica* B **241** 397–9

White W B 1974 *The Infrared Spectra of Minerals* (*Mineralogical Society Monograph* vol 4) ed V C Farmer (London: Mineralogical Society) pp 227–84 chapter 12

Wyckoff R W G 1963 *Crystal Structures* (New York: Wiley)